Helicity modulus and effective hopping in the two-dimensional Hubbard model using slave-boson methods

1995 J. Phys.: Condens. Matter 7 151

(http://iopscience.iop.org/0953-8984/7/1/014)

J. Phys.: Condens. Matter 7 (1995) 151–173. Printed in the UK

Helicity modulus and effective hopping in the two-dimensional Hubbard model using slave-boson methods

P J H Denteneer and M Blaauboer
Instituut-Lorentz, University of Leiden, PO Box 9506, 2300 RA Leiden, The Netherlands

Received 24 June 1994, in final form 6 October 1994

Abstract. The slave-boson mean-field method is used to study the two-dimensional Hubbard model. A magnetic phase diagram allowing for paramagnetism, weak and strong ferromagnetism and antiferromagnetism is constructed and compared to the corresponding phase diagram using the Hartree–Fock approximation (HFA). Magnetically ordered regions are reduced by a factor of about three along both the t/U and density axes compared to the HFA. Using the spin-rotation-invariant formulation of the slave-boson method the helicity modulus is computed and for half filling is found practically to coincide with that found using variational Monte Carlo calculations with the Gutzwiller wave function. Off half filling the results can be used to compare with quantum Monte Carlo calculations of the effective hopping parameter. Contrary to the case of half filling, the slave-boson approach is seen to greatly improve the results of the HFA when off half filling.

1. Introduction

In the study of correlated electrons, for which both charge and spin degrees of freedom are relevant, the Hubbard model is an intriguing simplification of reality that still contains a great deal of the essential physics [1]. Although superconductivity has not been demonstrated in this model, it is able to explain or reproduce a large number of experimental results on the copper oxides which superconduct at high temperatures [2]. Despite such encouraging results, understanding of the model in dimensions of two and higher is still rather limited. Even when the most elementary mean-field approximation, the Hartree–Fock approximation, is invoked, the phase diagram cannot be determined in full [3], since inhomogeneous phases, like spiral phases or domain walls, are able to supersede simple ferro- or antiferromagnetic phases. The possibility exists that more complicated phases not considered so far are also important. Rigorous techniques like quantum Monte Carlo and exact diagonalization are limited to temperatures which may be too high and lattices which may be too small, respectively. Therefore it is of interest to employ approximations which go beyond the Hartree–Fock approximation (HFA).

Some years ago Kotliar and Ruckenstein introduced, for the Hubbard model, the technique of using slave bosons to keep closer track of the site occupancy than is done in the HFA. If a further approximation is made, the so-called 'slave-boson mean-field' (SBMF) approximation, this approach was shown to be equivalent to the approximation scheme of Gutzwiller for the Hubbard model [4]. In a parallel development it was shown by Vollhardt and Metzner that the Gutzwiller approximation scheme becomes exact in the limit of an

0953-8984/95/010151+23$19.50

infinite number of spatial dimensions, whereas the HFA does not become exact in this limit [5, 6]. Therefore, just as in classical statistical physics, mean-field theory is a good starting point to study a specific model (because fluctuations become increasingly less relevant when increasing the dimension), for quantum models the SBMF approximation is a good starting point. In any case, it is expected to be an improvement over the HFA. In this connection, it is of interest to note that Oleś and Zaanen compared the Gutzwiller approximation (GA) with the HFA in a two-band model of copper oxide planes and showed that the GA is a good approximation for correlations at small length scales [7]. More recently the slave-boson approach of Kotliar and Ruckenstein has been refined in order to make it spin-rotation *invariant* [8, 9].

In this paper, we make a detailed comparison of the SBMF and Hartree–Fock approximations to the (one-band) Hubbard model on a two-dimensional square lattice. Where possible we also compare to quantum Monte Carlo calculations. By using the analytical result for the density of states of freely hopping electrons on the square lattice all calculations can conveniently be performed for a lattice of infinite size using one-dimensional integrals (over energy) only. Although we will mostly present results for the ground state ($T = 0$), the formulation we present is to a large extent valid for finite temperatures as well. A further advantage of the SBMF approach is that, in principle, it is valid for the whole range of Hubbard repulsion strengths and electron densities. First, we construct a ground-state phase diagram allowing only for the simple magnetic phases: paramagnetic, antiferromagnetic, weakly and strongly (i.e. partially and fully polarized) ferromagnetic. We determine all first-order and continuous transitions between these phases†. Although this approach may not give much information on the exact phase diagram (for instance, it is known that phases with spiralling magnetization supersede the antiferromagnet when going off half filling), it gives a clear impression of the improvement of the SBMF approximation over the HFA. Next, we derive an expression for the helicity modulus or spin stiffness in the SBMF approximation using the spin-rotation-invariant formulation and compare (for half filling) to previous calculations of the helicity modulus in the HFA, as well as using the Gutzwiller wave function in a variational Monte Carlo calculation [12, 14]. It turns out that in the SBMF approximation, apart from a negligible contribution, the helicity modulus is completely determined by the average kinetic energy (as is the case in the HFA) and therefore equivalent to the effective hopping parameter. When comparing the SBMF results for the effective hopping parameter to HFA and QMC calculations the improvement with respect to the HFA is only a few per cent at half filling and practically coincides with the results of variational Monte Carlo calculations using the Gutzwiller wave function, but the improvement is substantial off half filling.

The paper is organised as follows: in section 2, we briefly introduce the slave-boson mean-field method for the Hubbard model and present the free energy for the antiferromagnetic, ferromagnetic and spiral phases as well as the corresponding consistency equations. In section 3, we construct the ground-state phase diagram for the simple magnetic phases listed above and compare to the corresponding HFA phase diagram. An expression for the helicity modulus is derived and its connection to the effective hopping parameter is discussed in section 4. The SBMF results are compared to both the HFA and QMC calculations where possible. The last section contains a discussion of the results and draws some conclusions.

† Some of the results on the SBMF phase diagram were also obtained in [10]. A similar analysis using the Kotliar–Ruckenstein approach for the symmetric Anderson lattice model was given in [11].

2. Slave-boson mean-field method

The Hamiltonian for the Hubbard model is given by

$$\mathcal{H} = -\sum_{ij\sigma} t_{ij} c_{i\sigma}^{\dagger} c_{j\sigma} + U \sum_{i} n_{i\uparrow} n_{i\downarrow} - \mu \sum_{i\sigma} n_{i\sigma} \tag{1}$$

where $c_{i\sigma}^{\dagger}$ creates an electron at site i with spin σ, $n_{i\sigma} = c_{i\sigma}^{\dagger} c_{i\sigma}$, t_{ij} is the one-electron transfer integral between sites j and i (t_{ij} equals t if i and j are nearest neighbours and zero otherwise), U the on-site repulsion ($U > 0$), and μ the chemical potential ($\mu = U/2$ corresponds to a half-filled lattice, i.e. $n = \sum_{i\sigma} \langle n_{i\sigma} \rangle = 1$). The Hubbard model allows for four different occupancies of a single site: it can be empty, singly occupied by either a spin-up or spin-down electron or doubly occupied (by electrons of opposite spin). This leads to the idea of introducing four different kinds of 'slave' boson, one for each of the possible occupancies. In order for this to become a bookkeeping device one introduces the constraints that at each site there is always exactly one boson present and that it is of the kind corresponding to the electron occupancy. If e, $p_{\uparrow}$, $p_{\downarrow}$ and d denote the annihilation operators for the four kinds of boson, these constraints are

$$e_i^{\dagger} e_i + \sum_{\sigma} p_{i\sigma}^{\dagger} p_{i\sigma} + d_i^{\dagger} d_i = 1 \qquad \text{for all } i \tag{2}$$

$$c_{i\sigma}^{\dagger} c_{i\sigma} = p_{i\sigma}^{\dagger} p_{i\sigma} + d_i^{\dagger} d_i \qquad \text{for all } i \text{ and } \sigma = \uparrow, \downarrow. \tag{3}$$

The interaction term in the Hamiltonian (1) can now be replaced by one containing only the counting operator for d bosons. In order for the boson presence to keep in correspondence with the electron occupancy for each site, the hopping term in the Hamiltonian needs to be adjusted by connecting to each electron annihilation operator $c_{i\sigma}$ the following *boson-transformation* operator

$$\tilde{z}_{i\sigma} = e_i^{\dagger} p_{i\sigma} + p_{i,-\sigma}^{\dagger} d_i. \tag{4}$$

In fact this choice for $\tilde{z}$ is not unique [15] and we follow [4] by making a choice which in the case of $U = 0$ gives the correct result if a subsequent saddle-point approximation is made

$$z_{i\sigma} = \left(1 - d_i^{\dagger} d_i - p_{i\sigma}^{\dagger} p_{i\sigma}\right)^{-1/2} \tilde{z}_{i\sigma} \left(1 - e_i^{\dagger} e_i - p_{i,-\sigma}^{\dagger} p_{i,-\sigma}\right)^{-1/2}. \tag{5}$$

In the physical subspace, defined by (2) and (3), of the enlarged boson–electron Hilbert space, the Hamiltonian

$$\mathcal{H}_{\mathrm{SB}} = -\sum_{ij\sigma} t_{ij} c_{i\sigma}^{\dagger} z_{i\sigma}^{\dagger} z_{j\sigma} c_{j\sigma} + U \sum_{i} d_i^{\dagger} d_i - \mu \sum_{i\sigma} n_{i\sigma} \tag{6}$$

has the same matrix elements as the original Hamiltonian in the original Hilbert space containing only electron states. Therefore, up to here only a reformulation of the original problem has been achieved. However, if now in the functional integral formulation the saddle-point approximation of time- and position-independent Bose fields is made, a set of equations results which is similar to those found in the Hartree–Fock approximation, but more general. This approximation is called the slave-boson mean-field (SBMF) approximation. For comparison, the HFA can be obtained in such a functional integral formulation by first applying a suitable Hubbard–Stratonovich transformation and then making the saddle-point approximation for the original problem [16]. For further details on the functional integral formulation for the Hubbard model and the subsequent saddle-point approximation we refer to previous papers on this subject [4, 8, 9, 15, 17]. Here, we just

mention that the choice (5) is expected to be a reasonable choice also for larger U, since in the SBMF approximation it leads to the Gutzwiller approximation (see below), in which the density of doubly occupied sites is explicitly optimized. It is however by no means excluded that for very large U a better choice can be made by taking into account known properties of the model in this limit. Until now no proposals along these lines have been made. As a word of caution we mention that not only the non-uniqueness of (5), but also its explicit form, may lead to problems when going beyond the mean-field approximation by trying to include fluctuations. It has very recently been claimed that (5) is not a good starting point for treating fluctuations [18]. Since here we do not attempt to go beyond the mean-field level, we abstain from expanding on this problem.

In the next three subsections, we present the expressions for the free energy of the ferromagnetic, antiferromagnetic and spiral phases. Only for the spiral phase do we use explicitly the spin-rotationally invariant formulation of [17]. It turns out however that for the ferromagnetic and antiferromagnetic phases the invariant formulation reduces to the non-invariant formulation, so no generality is lost by using the non-invariant formulation from the outset for these phases. For the ferromagnet and antiferromagnet we also give the consistency equations for the appearing self-consistent fields, which must be obeyed for the free energy to become minimal. To some extent this is a repetition of previously published results [10, 17], but they are given for the reader's convenience and to establish the notation.

2.1. Ferromagnetic phase

For the ferromagnetic phase one assumes a non-zero homogeneous magnetization m, even if a magnetic field is absent. To be able to calculate the magnetic susceptibility we also include a magnetic field h in the Hamiltonians $\mathcal{H}$ and $\mathcal{H}_{\mathrm{SB}}$ by adding a term

$$\mathcal{H}_{\mathrm{mag}} = -h \sum_{i\sigma} \sigma n_{i\sigma}. \tag{7}$$

Here and in the following we adopt the convention that if σ does not appear as an index it attains the values $+1$ and -1 if the corresponding index is $\uparrow$ and $\downarrow$, respectively. In order to treat the density of electrons n and magnetization m on an equal footing, we introduce a slightly different definition for the free energy per site, to be denoted by φ. For the ferromagnet our free energy is defined as

$$\varphi_{\mathrm{F}} = -\frac{1}{\beta N} \ln \mathrm{Tr}\, \mathrm{e}^{-\beta(\mathcal{H}_{\mathrm{SB}}+\mathcal{H}_{\mathrm{mag}})} + \mu n + hm. \tag{8}$$

It is given by (see also [4, 10])

$$\varphi_{\mathrm{F}} = -\frac{1}{\beta N} \sum_{k,\sigma} \ln\left[1 + \mathrm{e}^{-\beta E_\sigma(k)}\right] + Ud^2 + \bar{\mu} n + \bar{\lambda} m \tag{9}$$

where

$$E_\sigma(k) = q_\sigma t(k) - \sigma\bar{\lambda} - \bar{\mu} \tag{10}$$

with

$$t(k) = -2t(\cos k_x + \cos k_y) \tag{11}$$

the band structure of freely hopping electrons on a square lattice. The density n and magnetization m are given by: $n = n_\uparrow + n_\downarrow$ and $m = n_\uparrow - n_\downarrow$ with $n_\sigma = \langle n_{i\sigma}\rangle$. Since in principle the electrons have been integrated out in obtaining (9), n and m can be understood

as a shorthand for the Bose fields $p_\uparrow$ and $p_\downarrow$ via the relation: $n_\sigma = p_\sigma^2 + d^2$ (which is the average of constraint (3)). The parameters $\bar{\mu}$ and $\bar{\lambda}$ are an effective chemical potential and effective magnetic field, respectively, which incorporate the Lagrange multipliers $\lambda_\sigma^{(2)}$ used to enforce the constraints (3)

$$\bar{\mu} = \mu - \tfrac{1}{2}\left(\lambda_\uparrow^{(2)} + \lambda_\downarrow^{(2)}\right) \tag{12}$$

$$\bar{\lambda} = h - \tfrac{1}{2}\left(\lambda_\uparrow^{(2)} - \lambda_\downarrow^{(2)}\right). \tag{13}$$

The Lagrange multiplier $\lambda^{(1)}$ associated with constraint (2) has disappeared because the average of this constraint must hold. In fact, both constraints are only satisfied on average in the saddle-point approximation. The band-renormalization factor q_σ appearing in (10) is in this approximation of time- and position-independent Bose fields a function of n, m and d (as follows directly from (4) and (5))

$$q_\sigma(n,m,d) \equiv \langle z_{j\sigma}^\dagger z_{i\sigma}\rangle = \frac{\left[\sqrt{(1-n+d^2)(n+\sigma m-2d^2)} + d\sqrt{n-\sigma m-2d^2}\right]^2}{(n+\sigma m)\left[1-\tfrac{1}{2}(n+\sigma m)\right]}. \tag{14}$$

We note that if this q_σ is rewritten as a function of $n_\uparrow, n_\downarrow$ and d one exactly recovers the expression for the band renormalization in the Gutzwiller approximation (see [19]; our d^2 is called d there†). This would not be true if another choice for $z_{i\sigma}$ than (5) had been made.

The sum over k in (9) is over the whole Brillouin zone of the square lattice. In the limit of an infinitely large lattice, which can be treated after the approximations made, the resulting integral over the (two-dimensional) Brillouin zone can be rewritten as an (one-dimensional) integral over energy using the density of states (DOS) of freely hopping electrons. For the square lattice this DOS, $\mathcal{N}(\varepsilon)$, is known analytically

$$\mathcal{N}(\varepsilon) \equiv \frac{1}{N}\sum_k \delta(\varepsilon - t(k)) = \begin{cases} (1/2\pi^2 t)K\left[1-(\varepsilon/4t)^2\right] & |\varepsilon| \leqslant 4t \\ 0 & |\varepsilon| > 4t \end{cases} \tag{15}$$

where $K(x)$ is the complete elliptic integral of the first kind [20]. Employing the DOS the free energy is

$$\varphi_F = -\frac{1}{\beta}\sum_\sigma \int \mathrm{d}\varepsilon\, \mathcal{N}(\varepsilon) \ln\left[1+\mathrm{e}^{-\beta E_\sigma(\varepsilon)}\right] + Ud^2 + \bar{\mu}n + \bar{\lambda}m \tag{16}$$

with $E_\sigma(\varepsilon) = q_\sigma\varepsilon - \sigma\bar{\lambda} - \bar{\mu}$. Unless explicitly stated otherwise integrals over ε run from $-\infty$ to ∞ (the relevant integration range is of course limited by (15)).

For a given interaction strength U, φ_F is now given as a function of the five variables $n, m, d, \bar{\mu}$ and $\bar{\lambda}$, whereas μ and h are control parameters, regulating (although not directly in this slave-boson approach) the density and magnetization. The optimal values for the five variables must be found from the three minimization conditions: $\partial\varphi_F/\partial d = 0$, $\partial\varphi_F/\partial\bar{\mu} = 0$, $\partial\varphi_F/\partial\bar{\lambda} = 0$, as well as from the two equations arising from the Legendre transform between grand potential (function of μ and h) and free energy (function of n and m): $\partial\varphi_F/\partial m = h$ and $\partial\varphi_F/\partial n = \mu$. Applying these conditions to (16) results in

$$U = -\frac{1}{2d}\sum_\sigma q_{\sigma d}\bar{\varepsilon}_\sigma \tag{17}$$

$$n = \sum_\sigma n_\sigma \tag{18}$$

† In [7] similar renormalization factors are derived in an alternative manner.

$$m = \sum_{\sigma} \sigma n_{\sigma} \tag{19}$$

$$\bar{\lambda} = h - \sum_{\sigma} q_{\sigma m} \bar{\varepsilon}_{\sigma} \tag{20}$$

$$\bar{\mu} = \mu - \sum_{\sigma} q_{\sigma n} \bar{\varepsilon}_{\sigma} \tag{21}$$

where $q_{\sigma\alpha}$ denotes the first partial derivative of q_{σ} with respect to α (= n, m, d) and we introduced the abbreviations

$$n_{\sigma} = \int \mathrm{d}\varepsilon \mathcal{N}(\varepsilon) f\left[E_{\sigma}(\varepsilon)\right] \tag{22}$$

$$\bar{\varepsilon}_{\sigma} = \int \mathrm{d}\varepsilon \mathcal{N}(\varepsilon) \varepsilon f\left[E_{\sigma}(\varepsilon)\right] \tag{23}$$

with the Fermi–Dirac distribution, $f(E) = \left[1 + \mathrm{e}^{\beta E}\right]^{-1}$. The five equations (17)–(21) need to be solved self-consistently for given U, μ and h and the results can be inserted in (16) to obtain the corresponding free energy. In practice, we will often be interested in calculations for a fixed density n, in which case the last equation (21) does not appear (μ disappears from the problem, however $\bar{\mu}$ remains). Expressions for partial derivatives of q_{σ} are given in appendix A.

The above allows us to compute the free energy of three different phases: the paramagnetic phase (PM), for which $m = 0$ if $h = 0$, the strong ferromagnet (SF), for which $m = n$ and both are non-zero even if $h = 0$, and the weak ferromagnet (WF), for which $m < n$ and both are non-zero even if $h = 0$. In section 3, we will obtain the lines in the $(t/U, n)$ diagram of first-order phase transitions between these phases. In order to obtain the line of the continuous phase transition between paramagnet and ferromagnet (the ferromagnet can be either strong or weak), one needs to find where the susceptibility χ of the paramagnet diverges. An expression for χ is derived in appendix B.

2.2. *Antiferromagnetic phase*

For the antiferromagnetic phase we divide the square lattice in two sublattices, such that points on one sublattice have only points of the other sublattice as nearest neighbours. Furthermore, we assume a non-zero staggered magnetization m_{s}, i.e. the magnetization is m_{s} on one sublattice and $-m_{\mathrm{s}}$ on the other. To be able to calculate the staggered susceptibility we add a staggered-magnetic-field term to the Hamiltonians $\mathcal{H}$ and $\mathcal{H}_{\mathrm{SB}}$:

$$\mathcal{H}_{\mathrm{mag,s}} = -\sum_{i\sigma} h_{i,s} \sigma n_{i\sigma} \tag{24}$$

where $h_{i,s}$ equals h_{s} on one sublattice and $-h_{\mathrm{s}}$ on the other. The saddle-point approximation of time- and position-independent Bose fields on each of the two sublattices separately (introducing staggered Lagrange multipliers as well) results in a 2×2 problem (for each σ separately, only one-electron states with k and $k + Q$ couple, $Q \equiv (\pi, \pi)$) for the quasiparticle spectrum, which is easily diagonalized. Analogously to the ferromagnet, we define the 'free energy' per site for the antiferromagnet as

$$\varphi_{\mathrm{AF}} = -\frac{1}{\beta N} \ln \mathrm{Tr}\, \mathrm{e}^{-\beta(\mathcal{H}_{\mathrm{SB}} + \mathcal{H}_{\mathrm{mag,s}})} + \mu n + h_{\mathrm{s}} m_{\mathrm{s}}. \tag{25}$$

It is given by

$$\varphi_{\mathrm{AF}} = -\frac{1}{\beta N} \sum_{k,\sigma}{}' \ln\left[1 + \mathrm{e}^{-\beta E(k)}\right] + U d^2 + \tilde{\mu} n + \tilde{\lambda}_{\mathrm{s}} m_{\mathrm{s}} \tag{26}$$

where

$$E(\boldsymbol{k}) = \pm\sqrt{q_s^2 t^2(\boldsymbol{k}) + \tilde{\lambda}_s^2} - \tilde{\mu} \tag{27}$$

and we have again introduced an effective chemical potential $\tilde{\mu}$ and an effective magnetic field $\tilde{\lambda}_s$. The prime indicates that the sum over $\boldsymbol{k}$ is over the magnetic Brillouin zone only ($k_x \pm k_y \in [-\pi, \pi]$). The band-renormalization factor q_s is now a σ-independent quantity because of the staggering

$$q_s(n, m_s, d) \equiv \langle z_{j\sigma}^{\dagger} z_{i\sigma} \rangle_{AF} = z_{A\sigma} z_{B\sigma} = z_\uparrow z_\downarrow \tag{28}$$

where

$$z_\sigma = \frac{\sqrt{(1-n+d^2)(n+\sigma m_s - 2d^2)} + d\sqrt{n-\sigma m_s - 2d^2}}{\sqrt{(n+\sigma m_s)\,(1-(n+\sigma m_s/2))}}. \tag{29}$$

As for the ferromagnet, the free energy can be expressed as an integral over the DOS of freely hopping electrons, $\mathcal{N}(\varepsilon)$

$$\varphi_{AF} = -\frac{1}{\beta}\int \mathrm{d}\varepsilon\, \mathcal{N}(\varepsilon) \ln\left[1 + \mathrm{e}^{-\beta E(\varepsilon)}\right] + Ud^2 + \tilde{\mu}n + \tilde{\lambda}_s m_s. \tag{30}$$

For convenience we restrict ourselves to densities $n \leqslant 1$; in that case only the negative square root in (27) is relevant and we have in (30)

$$E(\varepsilon) = -\sqrt{q_s^2\varepsilon^2 + \tilde{\lambda}_s^2} - \tilde{\mu}. \tag{31}$$

The consistency equations for the antiferromagnet are obtained in the same way as for the ferromagnet and read

$$U = \frac{q_{sd}}{2d}\bar{\varepsilon} \tag{32}$$

$$n = \int \mathrm{d}\varepsilon\, \mathcal{N}(\varepsilon) f[E(\varepsilon)] \tag{33}$$

$$m_s = \tilde{\lambda}_s \int \mathrm{d}\varepsilon \frac{\mathcal{N}(\varepsilon) f[E(\varepsilon)]}{\sqrt{q_s^2\varepsilon^2 + \tilde{\lambda}_s^2}} \tag{34}$$

$$\tilde{\lambda}_s = h_s + q_{sm_s}\bar{\varepsilon} \tag{35}$$

$$\tilde{\mu} = \mu + q_{sn}\bar{\varepsilon} \tag{36}$$

where we have defined

$$\bar{\varepsilon} = q_s \int \mathrm{d}\varepsilon \frac{\mathcal{N}(\varepsilon)\varepsilon^2 f[E(\varepsilon)]}{\sqrt{q_s^2\varepsilon^2 + \tilde{\lambda}_s^2}}. \tag{37}$$

Expressions for partial derivatives $q_{s\alpha}$ of q_s are given in appendix C. φ_{AF} is a function of the five variables n, m_s, d, $\tilde{\mu}$ and $\tilde{\lambda}_s$, whereas μ and h_s are control parameters. Calculating φ_{AF} for fixed U/t and n, means that the last consistency equation (36) becomes irrelevant again and the four remaining variables must be found self-consistently from the four remaining consistency equations. To compute the free energy the staggered field h_s is taken to be zero. This free energy may be compared to the free energies of the three phases discussed in the previous subsection and lines of first-order transitions in the $(t/U, n)$ plane may be found (see section 3). We note that the equations for the paramagnet can also be found from the above equations for the antiferromagnet by putting $m_s = 0$ if $h_s = 0$ (then also $\tilde{\lambda}_s = 0$). In order to find the transition line for the continuous phase transition between antiferromagnet and paramagnet an expression for the staggered susceptibility χ_s is derived in appendix D.

2.3. Spiral phase

To obtain the spiral phase the magnetization vector is assumed to vary in space as:

$$m_i = m\,(\cos(\boldsymbol{q}\cdot\boldsymbol{R}_i), \sin(\boldsymbol{q}\cdot\boldsymbol{R}_i), 0)\,. \tag{38}$$

In [17], the spin-rotation-invariant formulation is used to compute the free energy $\varphi_{\rm sp}$ for this phase. For details of this calculation we refer to [8, 17]; here it suffices to quote the result (in our notation)

$$\varphi_{\rm sp} = -\frac{1}{\beta N}\sum_{k,\nu}\ln\left[1+\mathrm{e}^{-\beta E_{q,\nu}(k)}\right] + Ud^2 + \breve{\mu}n - \lambda^{(2)}m \tag{39}$$

where

$$\begin{aligned} E_{q,\nu}(k) = {} & \left(z_+^2+z_-^2\right)\left[[t(k)+t(k+q)/2]\right] - \breve{\mu} \\ & + \nu\left\{\left(z_+^2-z_-^2\right)^2\left[[t(k)-t(k+q)/2]\right]^2\right. \\ & \left. + \left[z_+z_-[t(k)+t(k+q)]+\lambda^{(2)}\right]^2\right\}^{1/2} \end{aligned} \tag{40}$$

with $\nu = \pm 1$. The parameters $z_\pm$ are functions of n, m and d; in terms of the z_σ (formula (29) with m_s replaced by m) they are given by

$$z_\pm = \tfrac{1}{2}\left(z_\uparrow \pm z_\downarrow\right). \tag{41}$$

The parameter $\breve{\mu} = \mu - \lambda_0^{(2)}$ is again an effective chemical potential, whereas $\lambda_0^{(2)}$ and $\lambda^{(2)}$ are the Lagrange multipliers arising from the constraint (3) when made spin-rotation invariant†. We did not include any explicit magnetic field in the Hamiltonian in studying the spiral phases. One may verify that for $q = (0,0)$ and $q = (\pi,\pi)$, (40) reduces to the expressions (10) and (27) for the ferromagnet and antiferromagnet, respectively. In terms of the $z_\pm$ the band-renormalization factors are given by $q_\sigma = (z_+ + \sigma z_-)^2$ and $q_s = z_+^2 - z_-^2$.

For the spiral phase we do not give the consistency equations as we did for the ferromagnet and antiferromagnet, since we are only aiming at a simple phase diagram which does not include the spiral phases. Moreover, the consistency equations and free energy cannot be expressed as one-dimensional integrals over a density of states because of the spiralling vector q involved. Therefore, the consistency equations need to be solved numerically on a finite lattice. The regions in the phase diagram where spiral phases dominate the simple magnetic phases were calculated in [17] and [21]. In this paper, we will only use the expressions above to derive a formula within the SBMF approximation for the helicity modulus (or spin stiffness) and effective hopping parameter in section 4.

3. Magnetic phase diagram

We compute, in the SBMF approximation, the complete (i.e. all first-order and continuous phase transitions are included) ground-state magnetic phase diagram for the Hubbard model on a square lattice allowing for the four simple magnetic phases, paramagnet (PM), weak ferromagnet (WF), strong ferromagnet (SF) and antiferromagnet (AF). In their original paper, Kotliar and Ruckenstein [4] only calculated the lines where the PM becomes unstable towards ferromagnetic or antiferromagnetic ordering (continuous transitions), whereas Evans [10] also included some first-order transitions, but not all, so that an incomplete picture emerged.

† In the spin-rotation-invariant formulation, constraint (3) gives rise to a scalar Lagrange multiplier $\lambda_0^{(2)}$ as well as a vector Lagrange multiplier $\boldsymbol{\lambda}^{(2)}$. For a spiral phase the latter results in another scalar $\lambda^{(2)} = |\boldsymbol{\lambda}^{(2)}|$ because it must show the same spatial variation as m in (38).

First, the regions in the $(4t/U, n)$ plane where ferromagnetism (either WF or SF) and antiferromagnetism can occur are determined, by calculating the lines where the homogeneous and staggered susceptibilities, χ and χ_s, of the PM diverge. In appendices B and D expressions for χ and χ_s are derived. The condition that the denominator in these expressions vanishes (generalized Stoner criterion) provides an additional equation to be solved in conjunction with the consistency equations for the PM (see section 2.1). In this way, for fixed n, the additional equation fixes the (critical) U/t value for which the susceptibility diverges. The resulting lines are displayed in figure 1(a) and agree with previously published results [4, 10].

Now, using the formulae in sections 2.1 and 2.2 all first-order phase-transition lines in the $(4t/U, n)$ diagram are computed. Since no susceptibilities are required, h and h_s are taken to be zero. In principle, for each of the four phases for fixed values of U/t and n the energy is found by solving the consistency equations simultaneously†. For the SF and PM this problem simplifies somewhat: for the SF the set of equations (17)–(20) is reduced by one (since $m = n$) and for the PM we have $m = 0$. For each pair of phases one then finds a line in the $(4t/U, n)$ plane where the two energies are equal. The results of such calculations are displayed in figure 1(a). In principle there are six such lines, but the first-order PM/AF-transition line coincides with the continuous PM/AF transition. Note however that the continuous PM/F transition and the first-order PM/WF transition differ, implying that the magnetization in the WF phase does not vanish on the PM/WF-transition line (in contrast to the result of the Hartree–Fock approximation; see below).

Taking into account all four phases, the phase diagram of the Hubbard model on a square lattice in the SBMF approximation of figure 1(b) emerges, in which all interrupted lines denote first-order transitions and the full line a continuous (PM/AF) transition. We now discuss the phase diagram in comparison with the same phase diagram as obtained in the Hartree–Fock approximation (HFA) and in comparison with previously published SBMF results.

The corresponding, i.e., allowing for the same four phases, phase diagram to figure 1(b) in the HFA is shown in figure 1(c). A similar diagram was given previously in three dimensions by Penn [23] and in two dimensions by Hirsch [24], but in the latter the non-monotonic behaviour of the F/AF transition line was missed and the region of WF was not determined. Long has given the PM/F/AF phase diagram in HFA using a constant density of states; in that case no extremum in the F/AF transition occurs [25]. Another surprising feature of figure 1(c), besides the maximum in the F/AF line, is the fact that the WF/SF transition line is found to oscillate slightly around the line of the continuous P/F line. The difference in these curves is very small, but we have ascertained that it is *not* due to numerical inaccuracies. Thermodynamically such behaviour is allowed; it only means that along the P/F boundary the transition is sometimes continuous and sometimes first order. In comparing figure 1(b) and figure 1(c) it should be noted that they are topologically the same, but that because of the difference in scale on both the density and $4t/U$ axes, the SBMF has reduced the magnetically ordered regions considerably with respect to the HFA. Furthermore, the region where WF dominates has grown at the expense of the SF phase. In table 1, we list the location of the 'tripod' points (i.e., points where three phases meet; the AF/SF/WF and PM/SF/WF points are triple points, i.e., points where three first-order transitions meet), as well as the renormalization factor obtained in going from the HFA to the SBMF approximation. Globally speaking this factor is about three for the hole density δ and also

† Using the analytically known density of states (15) this may be conveniently done with the program MATHEMATICA [22]. Some care is required in integrating through the logarithmic singularity of $\mathcal{N}(\varepsilon)$ in $\varepsilon = 0$.

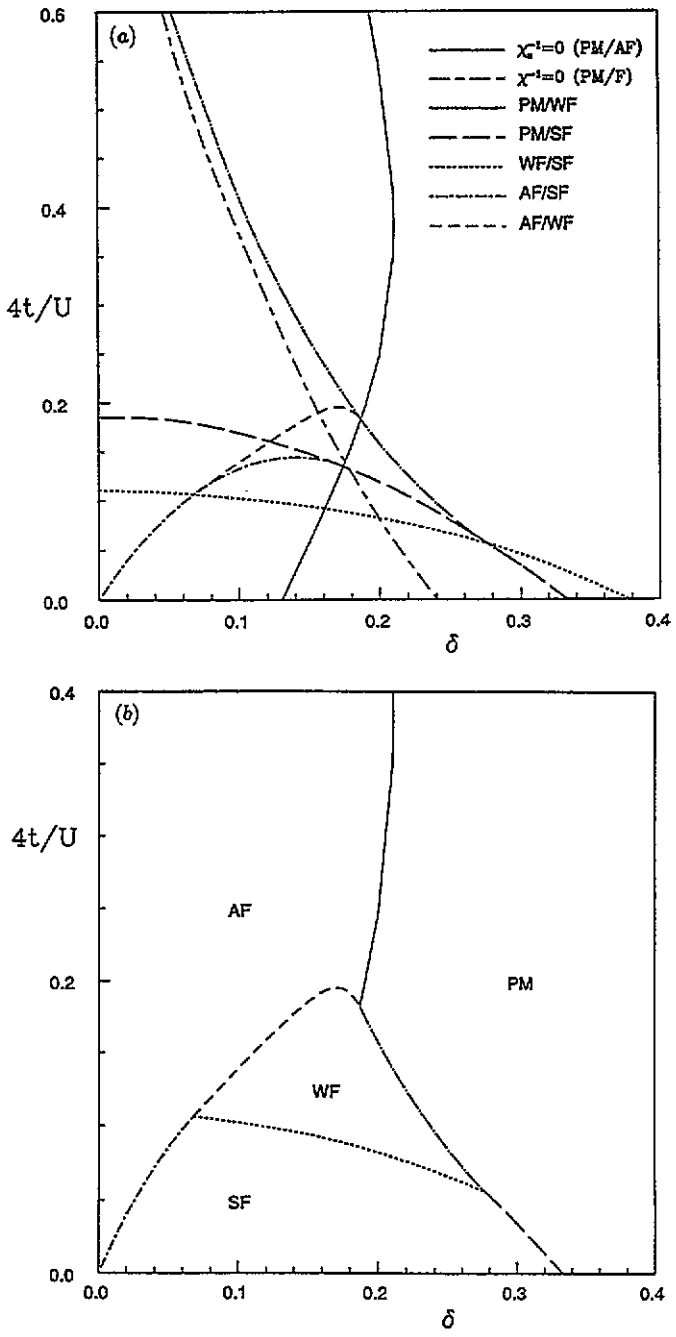

Figure 1. Ground-state $(4t/U, \delta)$ phase diagram of the Hubbard model on a square lattice, restricted to simple magnetic phases: paramagnet (PM), antiferromagnet (AF), weak (WF) and strong (SF) ferromagnet. δ is the density of holes: $1-n$. (a) Construction diagram showing all continuous and first-order transition lines obtained in the slave-boson mean-field approximation (SBMF), (b) phase diagram in the SBMF and (c) corresponding phase diagram in the Hartree–Fock approximation. Note the difference in scales of (b) and (c).

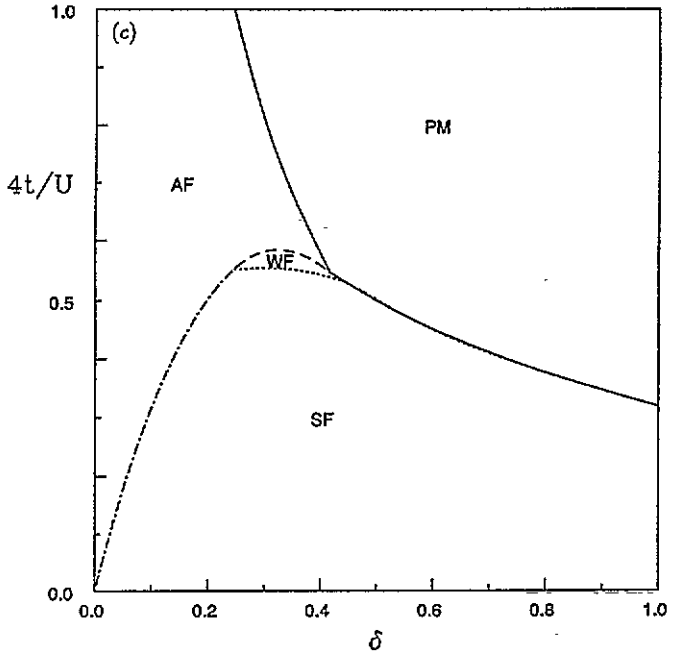

Figure 1. Continued.

about three for t/U (if the ferromagnetic region is considered as a whole). Since the HFA overestimates the importance of magnetic ordering [25], the SBMF approximation is clearly an improvement. The critical hole density above which antiferromagnetism cannot occur is determined by the continuous PM/AF transition and is given by $\delta_c^{AF} = 0.21$ in SBMF. More interestingly, the critical hole density above which ferromagnetism cannot occur is in SBMF determined by the first-order PM/SF transition and given by exactly $\delta_c^F = \frac{1}{3}$, as a simple argument can show (see e.g. [21]). The latter value agrees very well with the result $\delta_c^F = 0.29$ obtained from calculations using a variational wave function [26]. Remarkably, also high-temperature series expansions for the Hubbard model find for $U/t \to \infty$ a value of about 0.33, below which ferromagnetic nearest-neighbour correlations occur [27], and a value 'near $\frac{3}{11}$' ($\simeq 0.27$), below which a strong separation of energy scales for spin and translational degrees of freedom is observed [28]. Although these features in the high-temperature series expansions appear to be temperature independent over a wide temperature range, extrapolation to $T = 0$ is cumbersome in such expansions [29]. We also note that the $\chi^{-1} = 0$ line is nowhere in the diagram a phase boundary; therefore the continuous PM/F transition, in this approximation and contrary to the HFA result, is preempted by first-order PM/WF or PM/SF transitions.

A calculation of the phase diagram similar to ours was previously performed by Evans [10]. However, the more cumbersome PM/WF and AF/WF first-order transitions were not computed and for the WF/SF transition only the limit $m = n$ and $d = 0$ in the WF was taken. The latter determination turns out only to give an upper bound (in t/U, for fixed n) for the WF/SF first-order transition computed by comparing energies, as it should. As a result the final phase diagram of [10] is obtained by removing from figure 1(a) the PM/WF and AF/WF lines and replacing the WF/SF line by one extending from (0.15,0.0) to (0.0,0.38) in the $(4t/U, \delta)$ plane ($\delta = 1 - n$). Evans then appears to call WF only the tiny, triangle-shaped, region at the centre of our WF region (although this is not very clear from figure 1 in [10]).

Table 1. Comparison of location of tripod points (where three phases meet) in $(4t/U, \delta)$ phase diagram between Hartree–Fock approximation (HF) and slave-boson mean-field approximation (SBMF). Also the critical hole densities δ_c for antiferromagnetism (AF) and ferromagnetism (F) to occur in both approximations are compared. The last column gives the ratio of the HF and SBMF results in each case.

	SBMF	HF	HF/SBMF
$4t/U$			
AF/WF/SF	0.107	0.551	5.2
AF/WF/PM	0.183	0.548	3.0
WF/SF/PM	0.057	0.526	9.2
δ			
AF/WF/SF	0.067	0.25	3.7
AF/WF/PM	0.187	0.42	2.2
WF/SF/PM	0.275	0.45	1.6
δ_c			
AF	0.21	0.42	2.0
F	$\frac{1}{3}$	1	3.0

This assignment, however, is thermodynamically not justified since two of the boundaries then correspond to PM/SF and PM/AF transitions. Also the third boundary in that case (PM/F) is not a boundary for the WF region as computed by us.

To conclude the discussion of the phase diagram in figure 1, we stress that the actual ground-state phase diagram of the Hubbard model, even when constructed within either the HF or SBMF approximation, will also have to include inhomogeneous phases like domain walls and spiral phases. For instance, it was shown within the SBMF approximation that spiral phases supersede the antiferromagnet immediately when going off half filling and also the ferromagnetic phases shrink somewhat in favour of certain spiral phases [17, 21]. Our detailed determination of the simple phase diagram only serves to study the consequences of the SBMF approximation when compared with the HFA.

4. Helicity modulus and effective hopping

A crucial quantity in the study of quantum-ordered states is the helicity modulus, which is the stiffness associated with a twist of the order parameter, or, equivalently, with phase fluctuations of a complex order parameter. For the attractive Hubbard model, which exhibits superconducting or superfluid order, the helicity modulus corresponds to the superfluid density, whereas for the repulsive Hubbard model it is the spin stiffness of the AF ordered phase at half filling. In previous papers, the helicity modulus, denoted by ρ_s, was calculated for the 2D Hubbard model both in the HFA and by variational Monte Carlo methods [12, 13]. Also a comparison with exact diagonalization and quantum Monte Carlo results was made, showing that the HFA renders quantitatively reasonable results for ρ_s [14]. For the repulsive Hubbard model this could only be shown at half filling. Since we have already seen that the SBMF approximation is an improvement over the HFA, it is of interest to see what it will give for ρ_s. In this section, we first derive an expression for ρ_s within the SBMF approximation and use it to compute ρ_s. Then the connection between ρ_s and the effective hopping parameter is discussed, leading to calculations of the effective hopping both at half filling and off half filling. The SBMF results are compared to results from the HFA and quantum Monte Carlo results.

To obtain ρ_s, we can make use of the results for the spiral phase in section 2.3. In the

AF phase the order parameter is the staggered magnetization. This can be viewed as a spiral phase with spiral vector $q = Q \equiv (\pi, \pi)$. A small twist in the AF order parameter then corresponds to a spiral vector which deviates slightly from Q

$$q = (\pi, \pi) - \tilde{q}. \tag{42}$$

The helicity modulus ρ_s is given by

$$\rho_s = \lim_{\tilde{q}\to 0} \frac{\varphi(\tilde{q}) - \varphi(0)}{\frac{1}{2}\tilde{q}^2} \tag{43}$$

with the free energy per site φ given by (39) and where $\tilde{q}$ is the modulus of $\tilde{q}$. To facilitate the computation it is advantageous to perform a further manipulation. Since the spectrum is periodic in reciprocal space and we are going to integrate over the full Brillouin zone, it is allowed to shift the spectrum over $\frac{1}{2}\tilde{q}$, so that (40) becomes (if in turn we rename $\frac{1}{2}\tilde{q}$, for notational convenience, to q)

$$\begin{aligned} E_{q,\nu}(k) = {} & \left(z_+^2 + z_-^2\right)\left[t(k+q) - t(k-q)/2\right] - \breve{\mu} \\ & + \nu \Big\{ \left(z_+^2 - z_-^2\right)^2 \left[t(k+q) + t(k-q)/2\right]^2 \\ & + \left[z_+ z_- [t(k+q) - t(k-q)] + \lambda^{(2)}\right]^2 \Big\}^{1/2} \end{aligned} \tag{44}$$

with $\nu = \pm 1$. After this manipulation, the occurring sum $t(k+q) + t(k-q)$ is even in the small parameter q ($=|q|$) and the difference is odd. The same is not true for the small parameter $\tilde{q}$ in the occurring sum and difference $t(k) \pm t(k + Q - \tilde{q})$ in (40). In this notation, ρ_s is given by

$$\rho_s = \lim_{q\to 0} \frac{\varphi(q) - \varphi(0)}{2q^2}. \tag{45}$$

If we now restrict ourselves to ground-state properties ($T = 0$) and densities less than half filling ($n < 1$), we only need to expand the $\nu = -1$ branch for small q (and integrate over the Brillouin zone (BZ)) to obtain $\varphi(q) - \varphi(0)$ to order q^2. We find (taking $q = (q, 0)$ for convenience) that the term proportional to q vanishes after integrating over the BZ, and that ρ_s is given by

$$\rho_s = -\frac{t q_s^2}{N_s} \sum_k \left[\frac{t(k)\cos(k_x)}{2E(k)} + \frac{4 t z_+^2 z_-^2 t^2(k) \sin^2(k_x)}{E^3(k)} \right] \tag{46}$$

with

$$E(k) = \sqrt{q_s^2 t^2(k) + \lambda^2} \tag{47}$$

and the band renormalization q_s is

$$q_s = z_+^2 - z_-^2. \tag{48}$$

We have omitted the superscript (2) on λ. We remark that if the above shift in the BZ is not performed, a much longer expression for ρ_s results; the expression is equivalent to (46), but this is not trivial. We further note that the $T = 0$ HFA result of [12] is recovered by omitting the second term in the BZ sum and putting q_s equal to unity.

In order to compute ρ_s for fixed density n, according to section 2.2, the following set of equations needs to be solved self-consistently (for $T = 0$ and $h_s = 0$; cf. (32)–(35)):

$$m_s = 2\tilde{\lambda} \int_{\tilde{\mu}}^{4} \mathrm{d}\varepsilon \, \frac{\mathcal{N}(\varepsilon)}{\left(\varepsilon^2 + \tilde{\lambda}^2\right)^{1/2}} \tag{49}$$

$$\bar{\lambda} = \frac{2}{q_s} q_{sm_s} \int_{\bar{\mu}}^{4} d\varepsilon \, \frac{\mathcal{N}(\varepsilon)\varepsilon^2}{\left(\varepsilon^2 + \bar{\lambda}^2\right)^{1/2}} \tag{50}$$

$$U = \frac{q_{sd}}{d} \int_{\bar{\mu}}^{4} d\varepsilon \, \frac{\mathcal{N}(\varepsilon)\varepsilon^2}{\left(\varepsilon^2 + \bar{\lambda}^2\right)^{1/2}} \tag{51}$$

where $\bar{\lambda} = \lambda/q_s$ and $\bar{\mu}$ is determined by the fixed n

$$n = 2 \int_{\bar{\mu}}^{4} d\varepsilon \, \mathcal{N}(\varepsilon). \tag{52}$$

In terms of the parameters of section 2.2, we have $\bar{\mu} = \sqrt{\tilde{\mu}^2 - \tilde{\lambda}_s^2}/q_s$ ($\tilde{\lambda}_s$ is called λ here). The band renormalization q_s is given by (28) and (29). In terms of an integral over the DOS, the energy of the AF state (per site) and the spin stiffness ρ_s are given by

$$e_{AF} = -2q_s \int_{\bar{\mu}}^{4} d\varepsilon \, \mathcal{N}(\varepsilon)\sqrt{\varepsilon^2 + \bar{\lambda}^2} + Ud^2 + \bar{\lambda} q_s m_s \tag{53}$$

$$\rho_s = \frac{q_s}{4} \int_{\bar{\mu}}^{4} d\varepsilon \, \frac{\mathcal{N}(\varepsilon)\varepsilon^2}{\left(\varepsilon^2 + \bar{\lambda}^2\right)^{1/2}} - \frac{z_+^2 z_-^2}{q_s} \int_{\bar{\mu}}^{4} d\varepsilon \, \frac{\mathcal{N}_v(\varepsilon)\varepsilon^2}{\left(\varepsilon^2 + \bar{\lambda}^2\right)^{3/2}} \tag{54}$$

where $\mathcal{N}_v(\varepsilon)$ is the weighted density of states

$$\mathcal{N}_v(\varepsilon) \equiv \frac{1}{N} \sum_k \left[\nabla t(k)\right]^2 \delta(\varepsilon - t(k)) \tag{55}$$

which for a square lattice can be calculated analytically (see [30])

$$\mathcal{N}_v(\varepsilon) = \frac{8t}{\pi^2} \left\{ E\left[1 - \left(\frac{\varepsilon}{4t}\right)^2\right] - \left(\frac{\varepsilon}{4t}\right)^2 K\left[1 - \left(\frac{\varepsilon}{4t}\right)^2\right] \right\} \tag{56}$$

for $|\varepsilon| \leqslant 4t$ and zero otherwise. $K(x)$ and $E(x)$ are the complete elliptic integrals of the first and second kind, respectively. We remark that using the weighted density of states the finite-temperature result for ρ_s obtained in the HFA [12] can also be written as an integral over energy.

Table 2. Self-consistent parameters for antiferromagnetic ground state at half filling in slave-boson mean-field approximation as a function of U/t. The ground-state energy for $U/t = 0$ equals $-16/\pi^2$ exactly.

U/t	$\bar{\lambda}$	m_s	d	$-e_{AF}$	$q_s(1, m_s, d)$
0	0	0	0.5	1.62114	1
1	0.042	0.093 693	0.478 519	1.381 12	0.994 185
2	0.243 82	0.293 750	0.444 454	1.167 16	0.980 426
3	0.553 45	0.461 272	0.404 445	0.986 744	0.966 375
4	0.940 59	0.592 152	0.364 523	0.838 877	0.956 338
6	1.895 19	0.768 048	0.292 458	0.623 639	0.951 682
8	2.989 50	0.863 161	0.235 612	0.485 104	0.959 478
10	4.116 13	0.913 012	0.193 926	0.393 528	0.968 953
12	5.230 30	0.940 510	0.163 654	0.330 002	0.976 425
16	7.399 50	0.967 337	0.123 965	0.248 782	0.985 641
20	9.512 20	0.979 394	0.099 524	0.199 420	0.990 505
200.1	100	0.999 800	0.009 998	0.019 976	0.999 900

Since only at half filling is the AF phase the ground state, we first restrict ourselves to this case: $n = 1$ ($\bar{\mu} = 0$). In table 2, self-consistent parameters are given for various

U/t; the corresponding energy e_{AF} and band renormalization q_s are also given. These results agree with those published previously by Hasegawa [31]. In particular, we note that q_s never deviates from unity by more than 5%, implying that slave bosons at half filling renormalize the Hartree–Fock results only by a small amount. As concerns ρ_s, for the case of half filling the integral containing $\mathcal{N}_v(\varepsilon)$ plays no role since for $n = 1$ we have $z_- = 0$ (as is easily verified from (29) and (41)). In table 3 and figure 2, we compare the results for ρ_s obtained in the SBMF with those obtained previously using the HFA and using variational Monte Carlo calculations with an (antiferromagnetic) Gutzwiller wave function (GWVMC) [12]. The fact that slave bosons only renormalize the HF results a little is reflected in the fact that the SBMF and HF results never differ by more than 7%. Note however that the SBMF result is always larger (except for very small U/t, $U/t < 2.5$), whereas q_s, which enters as a factor in (54), is smaller than unity. The direct effect of q_s is more than compensated by a renormalized (smaller) value of the antiferromagnetic gap $\lambda = \bar{\lambda} q_s$. A further observation from table 3 and figure 2 is that the SBMF results almost coincide with the GWVMC results. The difference between the results is an indication of the difference between the Gutzwiller *approximation* (which is equivalent to the present SBMF approximation, see the introduction) and the Gutzwiller *wave function*. Although these are not identical [6], the difference for the spin stiffness is not big, as shown in figure 2. Therefore the tedious variational Monte Carlo calculations for ρ_s can be replaced by the above set of equations which are exact (within the SBMF) and easy to solve.

Table 3. Spin stiffness ρ_s of the antiferromagnetic ground state at half filling as a function of U/t as calculated in the Hartree–Fock approximation (HFA), the slave-boson mean-field approximation (SBMF) and from variational Monte Carlo calculations using the Gutzwiller wavefunction (GWVMC). For $U/t = 0$, ρ_s equals $2/\pi^2$ exactly. For HFA and SBMF, results are for an infinitely large lattice; for GWVMC, results are for an 8×8 lattice, except for $U/t = 2, 3$ which are for 20×20 and 14×14 lattices, respectively (see also [12]).

U/t	ρ_s^{HFA}	ρ_s^{SBMF}	ρ_s^{GWVMC}
0	0.2026	0.2026	—
1	0.2023	0.2012	—
2	0.1960	0.1953	0.197
3	0.1820	0.1847	0.185
4	0.1650	0.1713	0.172
6	0.1332	0.1421	0.141
8	0.1090	0.1162	0.117
10	0.0912	0.0962	0.098
12	0.0781	0.0814	0.083
16	0.0602	0.0618	—
20	0.0488	0.0497	—

On very general grounds it can be derived that the helicity modulus (spin stiffness for positive U and superfluid weight for negative U) comprises a 'direct' part proportional to the average kinetic energy $\langle T \rangle$ and a part related to the current–current correlation function Λ_{xx} [32]. The HFA effectively neglects the Λ_{xx} part, whereas GWVMC calculations find only a negligible correction to the kinetic part $-\frac{1}{8}\langle T \rangle$ [12]. Since in formula (46) the first term is exactly $-\frac{1}{8}\langle T \rangle$ in the SBMF approximation and at half filling the second term equals zero, we can conclude that also the SBMF approximation only gives the kinetic part of ρ_s. In [14] it was estimated (by comparing to appropriate exact diagonalization calculations and quantum Monte Carlo (QMC) calculations) that the HFA overestimates ρ_s at half filling by 68%, 40%,

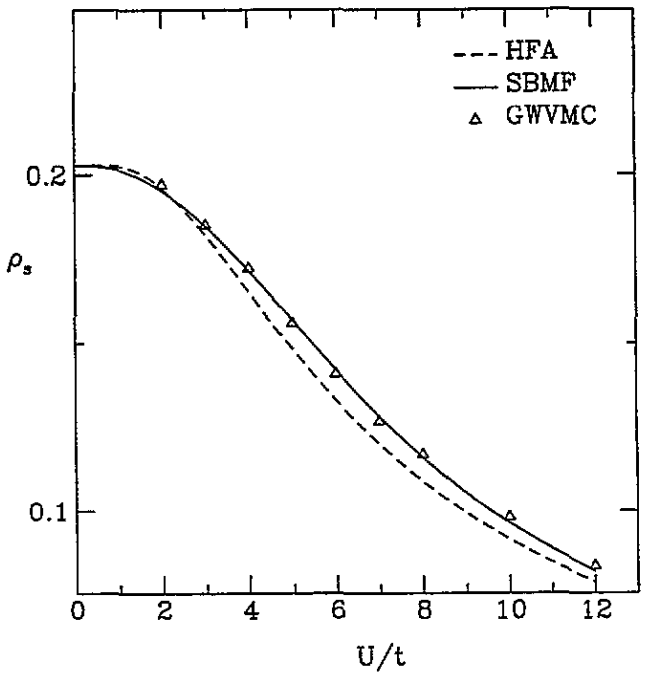

Figure 2. Helicity modulus ρ_s for the repulsive Hubbard model on a square lattice at half filling as a function of U/t. Shown are results from the Hartree–Fock approximation (HFA), from the slave-boson mean-field approximation (SBMF) and from variational Monte Carlo calculations using a Gutzwiller projected wave function (GWVMC, from [12]).

38% and 36% for $U/t = 4$, 8, 10 and 20, respectively. However, if one compares the kinetic energy found in the HF and SBMF approximations with QMC calculations for $n = 1$ (the latter are obtained from [34]), one concludes that the approximations perform very satisfactorily. This is illustrated in figure 3, where we plot the effective hopping integral t_{eff}, defined by normalizing the average kinetic energy for interaction constant U with that for $U = 0$

$$\frac{t_{\text{eff}}}{t} = \frac{\langle c^\dagger_{i\sigma} c_{j\sigma} + c^\dagger_{j\sigma} c_{i\sigma} \rangle_U}{\langle c^\dagger_{i\sigma} c_{j\sigma} + c^\dagger_{j\sigma} c_{i\sigma} \rangle_{U=0}}. \tag{57}$$

The denominator is easily evaluated as the energy of the PM phase in the HFA, since for $U = 0$ the HFA is exact and there is no potential energy. The QMC data are taken at sufficiently low temperature ($\beta t = 16$) for this comparison with $T = 0$ results to be meaningful. We note that a similar comparison of SBMF and QMC data was made in [33]; in that paper the SBMF approach was formulated as a 14-dimensional optimization problem. By comparing their figure 2(b) with our figure 3, the results from our simple formula (54) are found to be the same. A surprising feature of figure 3 is perhaps not so much that the SBMF results approximate the QMC results so well, but that the HFA results do the same already.

We now discuss the off-half-filling case; since off half filling there exists a spiralling vector q_0 for which the spiral phase has lower energy than the AF phase, we cannot call ρ_s as given by (54) the stiffness of the ground state any longer. Instead, the expression (54) has the interpretation of the stiffness of the AF phase with respect to a small deviation from spiralling vector (π, π). In order to compute the stiffness of the ground state one would have to perturb the spiral phase with vector q_0, but this is beyond the scope of the present paper. Here we only investigate how well the effective hopping (or, equivalently,

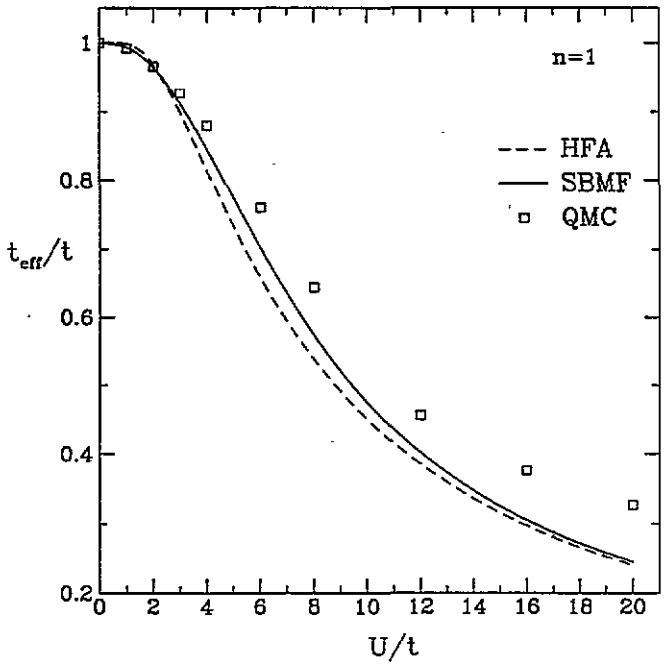

Figure 3. Effective hopping integral $t_{\rm eff}/t$ for the repulsive Hubbard model on a square lattice at half filling as a function of U/t. Shown are results from the Hartree–Fock approximation (HFA), the slave-boson mean-field approximation (SBMF) and quantum Monte Carlo calculations (QMC, from [34]).

the kinetic energy) of the two-dimensional Hubbard model off half filling is described by the first term in (54). In figure 4(a), we compare $t_{\rm eff}/t$ obtained from Hartree–Fock and SBMF approximations (for $T = 0$) with low-temperature ($\beta t = 6$) QMC data (the latter are obtained from [35]). The results are displayed as a function of density n for the one value of U/t (=4) for which there are QMC data available. From the phase diagrams in figure 1 it is clear that in both the HFA and SBMF approximation an AF/PM transition occurs† for some critical density n_c ($n_c = 0.86$ in SBMF and $n_c = 0.76$ in HFA for $U/t = 4$, the former is not shown in figure 1(a)). Below n_c (paramagnetic phase), $t_{\rm eff}/t$ equals unity in the HFA and equals the band renormalization q ($=q_\uparrow = q_\downarrow$) in the SBMF approximation. Clearly the SBMF approach is a significant improvement over the HFA; the agreement with the QMC data is less good in the density interval just off half filling. This is most probably caused by the fact that for these densities the assumed (antiferromagnetic) phase in the SBMF approach is not the correct one. The same remark concerning [33] as made above for $n = 1$ is appropriate here. Finally, in figure 4(b), we also show the results for the effective hopping integral for a few other values of U/t, for which no QMC data are available. The corresponding HFA curves are not shown, but the behaviour is similar to that for $U/t = 4$: at half filling $t_{\rm eff}/t$ is somewhat below the SBMF result and rises to unity in going off half filling. The densities below which $t_{\rm eff}/t$ equals unity can be read off from figure 1(c). We note that in figure 4(b) the non-differentiability at n_c (which is close to 0.8 for $U/t = 8, 12, 16$, as can be seen in figure 1(a) and (b)) is less pronounced for $U/t = 8, 12, 16$ than it is for $U/t = 4$.

† If the restricted set of four phases is considered as before.

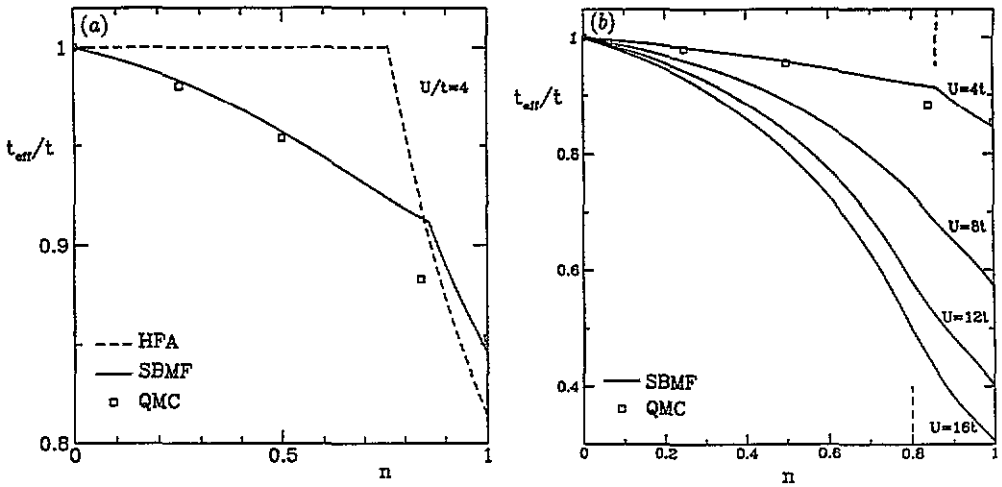

Figure 4. Effective hopping integral $t_{\rm eff}/t$ for the repulsive Hubbard model on a square lattice as a function of electron density n. (a) For $U/t = 4$, results are shown from the Hartree–Fock approximation (HFA), the slave-boson mean-field approximation (SBMF) and quantum Monte Carlo calculations (QMC, from [35]), and (b) for $U/t = 4$, 8, 12, and 16 from SBMF calculations (QMC results for $U/t = 4$ only). The dashed lines indicate the electron densities $n_{\rm c}$ for which in the phase diagram in figure 1(a) a continuous PM/AF transition takes place. For $U/t = 8$, 12 and 16 the value of $n_{\rm c}$ is (approximately) equal to 0.8 in each case.

5. Discussion and conclusions

Above we have given a detailed account of calculations within the slave-boson mean-field (SBMF) approximation for the repulsive Hubbard model on a square lattice. We have focused on the phase diagram, a particular response function, the helicity modulus $\rho_{\rm s}$ and the related effective hopping integral. All calculations can be expressed in terms of a set of integral equations with one-dimensional integrals over energy containing a density of states, which is known analytically for the square lattice. These equations are solved self-consistently.

If for the $(t/U, n)$ phase diagram we restrict ourselves to simple magnetic phases, the SBMF approach is found to reduce the magnetically ordered regions with respect to the Hartree–Fock approximation (HFA). Along the density axis the reduction is roughly a factor of three, whereas along the t/U axis the reduction of the ferromagnetic region (weak and strong ferromagnetism together) is also a factor of three. In the SBMF approach the portion of weak ferromagnetism grows at the expense of the strong-ferromagnetism portion when compared to the HFA. The present SBMF phase diagram is more likely to be a good starting point for more sophisticated approaches to the phase diagram than is the HFA phase diagram, because in an infinite number of dimensions the SBMF approach becomes exact (see the introduction). On the other hand, it is seen that the SBMF approach is not qualitatively different from the HFA, but rather a renormalized form of HFA.

The new quantity that we obtain within the SBMF approach is the helicity modulus $\rho_{\rm s}$. At half filling, the results for $\rho_{\rm s}$ practically coincide with those obtained using variational Monte Carlo calculations with a Gutzwiller wave function and are generally somewhat larger (about 5%) than those obtained in the HFA. The exact results are estimated to be smaller than the HFA results. This discrepancy is due to the neglect within the SBMF approach (as in the HFA) of the current–current correlation part of $\rho_{\rm s}$. The remaining *kinetic part* of $\rho_{\rm s}$ agrees very well with quantum Monte Carlo (QMC) calculations of the kinetic energy

or effective hopping integral. Also off half filling, where our expression for ρ_s no longer has the interpretation of helicity modulus of the ground state, it is found to represent the effective hopping much better than the HFA.

A number of extensions of the present work are possible. Most of the extensions discussed below have already been performed within the HFA [12] and since the SBMF approach turns out to be a renormalized form of the HFA, the qualitative effect of such expansions on the present SBMF results can be predicted. A possible sequel to the present work (which was not attempted before for the HFA) is the calculation of the helicity modulus for the spiral or domain-wall phases, which supersede the AF ground state that one has at half filling and which is the starting point for our calculated helicity modulus. Another extension is to introduce a homogeneous magnetic field h in the AF phase at half filling. Using the well known mapping between repulsive and attractive Hubbard models (see e.g. [12]) the corresponding expression for ρ_s then equals the superfluid density of the attractive ($U < 0$) Hubbard model off half filling (without a magnetic field). A final straightforward but tedious extension of the present results is to allow for finite temperatures. The formalism set up above is perfectly capable of dealing with this more general case, but the calculations become somewhat more tedious than for $T = 0$. Furthermore, the interpretation of the SBMF phase diagram becomes more cumbersome for finite T, since ordered phases will continue to exist up to some critical temperature, whereas long-range order is not allowed in the exact solution in two dimensions because of the Mermin–Wagner theorem [36].

Acknowledgments

We acknowledge discussions with J M J van Leeuwen, J Zaanen and M L Horbach on various aspects of the work presented in this paper.

Appendix A. Band-renormalization factor q_σ

In this appendix expressions for partial derivatives of the band-renormalization factor q_σ for the ferromagnet are given. The formula for q_σ, which is a function of density n, magnetization m and density of doubly occupied sites d^2, is repeated here (see (14))

$$q_\sigma(n,m,d) \equiv \langle z_{j\sigma}^\dagger z_{i\sigma}\rangle = \frac{\left[\sqrt{(1-n+d^2)(n+\sigma m-2d^2)}+d\sqrt{n-\sigma m-2d^2}\right]^2}{(n+\sigma m)\left[1-\frac{1}{2}(n+\sigma m)\right]}. \tag{A1}$$

For n, m and d in the physically relevant range (e.g., m should be less than or equal to n and d^2 should be less than or equal to $\frac{1}{2}n$) q_σ attains values between zero and unity, so the free electron bands are *narrowed* in the SBMF approximation.

First partial derivatives $q_{\sigma n}$, $q_{\sigma m}$ and $q_{\sigma d}$ with respect to n, m and d, respectively, are

$$q_{\sigma n} = \frac{N_\sigma}{D_\sigma}\left[\frac{e}{r_\sigma}-\frac{r_\sigma}{e}+\frac{d}{r_{-\sigma}}\right]-\frac{N_\sigma^2}{D_\sigma^2}(1-n-\sigma m) \tag{A2}$$

$$q_{\sigma m} = \sigma\frac{N_\sigma}{D_\sigma}\left[\frac{e}{r_\sigma}-\frac{d}{r_{-\sigma}}\right]-\sigma\frac{N_\sigma^2}{D_\sigma^2}(1-n-\sigma m) \tag{A3}$$

$$q_{\sigma d} = 2d\frac{N_\sigma}{D_\sigma}\left[\frac{r_\sigma}{e}-\frac{2e}{r_\sigma}+\frac{r_{-\sigma}}{d}-\frac{2d}{r_{-\sigma}}\right] \tag{A4}$$

where we have introduced the abbreviations

$$N_\sigma = \sqrt{(1-n+d^2)(n+\sigma m-2d^2)}+d\sqrt{n-\sigma m-2d^2} \tag{A5}$$

$$D_\sigma = n + \sigma m - \tfrac{1}{2}(n + \sigma m)^2 \tag{A6}$$

$$e = \sqrt{1 - n + d^2} \tag{A7}$$

$$r_\sigma = \sqrt{n + \sigma m - 2d^2}. \tag{A8}$$

To determine where the susceptibility diverges (see appendix B), we also require q_{mm}, the second derivative of q_σ with respect to m calculated at $m = 0$ (which is independent of σ)

$$q_{mm} = \frac{N_0^2}{D_0^2}\left[1 + \frac{2(1-n)^2}{D_0}\right] - \frac{2(1-n)^2}{D_0^2} - \frac{2ed}{(n-2d^2)D_0} \tag{A9}$$

with

$$N_0 = \sqrt{n - 2d^2}\left(\sqrt{1 - n + d^2} + d\right) \tag{A10}$$

$$D_0 = n(1 - n/2). \tag{A11}$$

Appendix B. Homogeneous magnetic susceptibility for paramagnet

In this appendix we derive a formula for the homogeneous magnetic susceptibility χ in the paramagnetic phase:

$$\chi \equiv \left(\frac{\partial m}{\partial h}\right)_{h=0}. \tag{B1}$$

The derivation proceeds as follows: in the paramagnet, we have $m = 0$ if $h = 0$ in the equations (17)–(21) of section 2.1. Then also $\bar{\lambda} = 0$. The solutions of the consistency equations of the remaining variables we call n_0, d_0 and $\bar{\mu}_0$. Now we apply an infinitesimal magnetic field δh. Then m and $\bar{\lambda}$ will acquire small non-zero values δm and $\delta\lambda$ and the other quantities will deviate slightly from their values for $h = 0$, because all are coupled through (17)–(21). If we now work at a fixed density (i.e., n is not allowed to deviate from n_0 and equation (21) becomes irrelevant), we have four equations containing five small quantities. From these the required ratio $\partial m/\partial h$ is obtained. Working out this procedure, by expanding all equations to first order in the small quantities, it turns out (perhaps not surprisingly) that the equations for $\delta\bar{\mu}$ and δd decouple from those for δm, $\delta\lambda$ and δh. Here we give the equations for the latter three quantities for the case $T = 0$ (for which the derivative of the Fermi–Dirac distribution is a convenient delta-function)

$$\delta m = a\delta m + \chi_0 \delta\lambda \tag{B2}$$

$$\delta\lambda = \delta h + b\delta m + a\delta\lambda \tag{B3}$$

where we have introduced the following notation

$$\chi_0 = \frac{2\mathcal{N}_F}{q} \tag{B4}$$

$$a = -\frac{2\mathcal{N}_F q_m \bar{\mu}_0}{q^2} \tag{B5}$$

$$b = -2q_{mm}\bar{\varepsilon}_0 + \frac{2\mathcal{N}_F q_m^2 \bar{\mu}_0^2}{q^3} \tag{B6}$$

with

$$\mathcal{N}_F = \mathcal{N}(\bar{\mu}_0/q) \tag{B7}$$

$$\bar{\varepsilon}_0 = \int_{-\infty}^{\bar{\mu}_0/q} \mathrm{d}\varepsilon\, \mathcal{N}(\varepsilon)\varepsilon \tag{B8}$$

and q and q_m are the functions q_σ and $q_{\sigma m}$ taken at $m = 0$ (see appendix A). Solving (B2) and (B3) for χ finally gives the required formula for the susceptibility

$$\chi = \frac{\chi_0}{(1-a)^2 - b\chi_0}. \tag{B9}$$

A similar result was given in [10], although there is a factor of two difference in the $\bar{\varepsilon}_0$ term in (B6).

Appendix C. Band-renormalization factor q_s

In this appendix expressions for partial derivatives of the band-renormalization factor q_s for the antiferromagnet are given. The formula for q_s, which is a function of density n, staggered magnetization parameter m_s and density of doubly occupied sites d^2, is repeated here (cf. (28) and (29))

$$q_s(n, m_s, d) = z(n, m_s, d)z(n, -m_s, d)\ , \tag{C1}$$

where

$$z(n, m_s, d) = \frac{\sqrt{(1-n+d^2)(n+m_s-2d^2)} + d\sqrt{n-m_s-2d^2}}{\sqrt{(n+m_s)\,(1-(n+m_s/2))}}. \tag{C2}$$

Introducing the abbreviations $N_\pm$ and the partial derivative of z with respect to m_s

$$N_\pm = \sqrt{(n \pm m_s)\left(1 - \frac{n \pm m_s}{2}\right)} \tag{C3}$$

$$\frac{\partial z}{\partial m_s} = \frac{1}{2N_+}\left\{\sqrt{\frac{1-n+d^2}{n+m_s-2d^2}} - \frac{d}{\sqrt{n-m_s-2d^2}} - \frac{z(n, m_s, d)}{N_+}[1-n-m_s]\right\} \tag{C4}$$

the first partial derivatives with respect to m_s and d are (since we always work at fixed density, the derivative with respect to n is not needed):

$$q_{sm_s} = z(n, -m_s, d)\frac{\partial z(n, m_s, d)}{\partial m_s} + z(n, m_s, d)\frac{\partial z(n, -m_s, d)}{\partial m_s} \tag{C5}$$

$$q_{sd} = \frac{4d}{N_+N_-}\left\{\frac{(n-2d^2)(2n-1-4d^2) - m_s^2}{\sqrt{n^2 - m_s^2 - 4nd^2 + 4d^4}} + \frac{(1-n)n - 8d^4 + (8n-6)d^2}{2d\sqrt{1-n+d^2}}\right\}. \tag{C6}$$

For the calculation of the staggered susceptibility (see appendix D) the second derivative of q_s with respect to m_s at $m_s = 0$ is required; the formula is

$$q_{m_sm_s} \equiv \left(\frac{\partial^2 q_s}{\partial m_s^2}\right)_{m_s=0} = \frac{4n^2 - 8n + 8}{n^3(2-n)^3}\left[\sqrt{1-n+d^2} + d\right]^2(n-2d^2) - \frac{2(1-n+2d^2)}{n(2-n)(n-2d^2)}. \tag{C7}$$

Appendix D. Staggered magnetic susceptibility for the paramagnet

In this appendix we derive a formula for the staggered magnetic susceptibility in the paramagnetic phase χ_s:

$$\chi_s \equiv \left(\frac{\partial m_s}{\partial h_s}\right)_{h_s=0}. \tag{D1}$$

The procedure is as follows: the consistency equations (32)–(36) for the antiferromagnet in section 2.2 allow for a paramagnetic solution in which $h_s = 0$ leads to $m_s = 0$ as well as $\tilde{\lambda}_s = 0$. Starting from this solution, we apply (at a fixed density) an infinitesimal staggered magnetic field δh_s. This introduces small changes in the other parameters in particular m_s and $\tilde{\lambda}_s$ acquire small values δm_s and $\delta\tilde{\lambda}_s$ (the changes in d and $\tilde{\mu}$ are irrelevant for the present discussion). Restricting ourselves to the $T = 0$ case, the two equations relating δh_s, δm_s and $\delta\tilde{\lambda}_s$ are (expanding the consistency equations to first order in δh_s, δm_s and $\delta\tilde{\lambda}_s$)

$$\delta m_s = \chi_{s,0}\,\delta\tilde{\lambda}_s \tag{D2}$$

$$\delta\tilde{\lambda}_s = \delta h_s + b_s\,\delta m_s \tag{D3}$$

where the following abbreviations are introduced

$$\chi_{s,0} = \frac{2}{q}\int_{-\infty}^{-\tilde{\mu}/q} \mathrm{d}\varepsilon\,\frac{\mathcal{N}(\varepsilon)}{\varepsilon} \tag{D4}$$

$$b_s = 2q_{m_s m_s}\int_{-\infty}^{-\tilde{\mu}/q} \mathrm{d}\varepsilon\,\mathcal{N}(\varepsilon)\varepsilon. \tag{D5}$$

Here the parameter q is q_s taken at $m_s = 0$ (see appendix C). Solving (D2) and (D3) for χ_s one has

$$\chi_s = \frac{\delta m_s}{\delta h_s} = \frac{\chi_{s,0}}{1 - b_s\chi_{s,0}}. \tag{D6}$$

A similar result was obtained in [10].

References

[1] Hubbard J 1963 *Proc. R. Soc.* A **276** 238
Gutzwiller M C 1963 *Phys. Rev. Lett.* **10** 159
Kanamori J 1963 *Prog. Theor. Phys.* **30** 275
Anderson P W 1959 *Phys. Rev.* **115** 2
[2] Dagotto E 1994 *Rev. Mod. Phys.* to be published
[3] Inui M and Littlewood P B 1991 *Phys. Rev.* B **44** 4415
[4] Kotliar G and Ruckenstein A E 1986 *Phys. Rev. Lett.* 57 1362
[5] Metzner W and Vollhardt D 1989 *Phys. Rev. Lett.* **62** 324
[6] Vollhardt D 1992 *Proc. Enrico Fermi Summer School (Varenna)*
[7] Oleś A M and Zaanen J 1989 *Phys. Rev.* B **39** 9175
[8] Li T, Wölfle P and Hirschfeld P J 1989 *Phys. Rev.* B **40** 6817
[9] Frésard R and Wölfle P 1992 *Int. J. Mod. Phys.* B **6** 685; erratum **6** 3087
[10] Evans S M M 1992 *Europhys. Lett.* **20** 53
[11] Dorin V and Schlottmann P 1993 *Phys. Rev.* B 47 5095
[12] Denteneer P J H, An Guozhong and van Leeuwen J M J 1993 *Phys. Rev.* B 47 6256
[13] Denteneer P J H, An Guozhong and van Leeuwen J M J 1991 *Europhys. Lett.* **16** 5
[14] Denteneer P J H 1994 *Phys. Rev.* B **49** 6364
[15] Lavagna M 1990 *Phys. Rev.* B **41** 142
[16] Fradkin E 1991 *Field Theories of Condensed Matter Systems* (Reading, MA: Addison-Wesley)
[17] Frésard R and Wölfle P 1992 *J. Phys.: Condens. Matter* 4 3625
[18] Arrigoni E and Strinati G C 1993 *Phys. Rev. Lett.* **71** 3178
Arrigoni E, Castellani C, Grilli M, Raimondi R and Strinati G C 1994 *Phys. Rep.* **241** 291
[19] Vollhardt D 1984 *Rev. Mod. Phys.* **56** 99
[20] Abramowitz M and Stegun I A (ed) 1970 *Handbook of Mathematical Functions* (New York: Dover)
[21] Möller B, Doll K and Wölfle P 1993 *J. Phys.: Condens. Matter* **5** 4847
[22] Wolfram S 1991 *MATHEMATICA, a system for Doing Mathematics by Computer* (Reading MA: Addison-Wesley)
[23] Penn D R 1966 *Phys. Rev.* **142** 350
[24] Hirsch J E 1985 *Phys. Rev.* B **31** 4403
[25] Long M W 1991 *The Hubbard Model: Recent Results* ed M Rasetti (Singapore: World Scientific)

[26] von der Linden W and Edwards D M 1991 *J. Phys.: Condens. Matter* **3** 4917
[27] ten Haaf D F B and van Leeuwen J M J 1992 *Phys. Rev.* B **46** 6313
[28] Yedidia J S 1990 *Phys. Rev.* B **41** 9397
[29] ten Haaf D F B, Brouwer P W, Denteneer P J H and van Leeuwen J M J 1994 *Phys. Rev.* B at press
[30] Belkhir L and Randeria M 1994 *Phys. Rev.* B **49** 6829
[31] Hasegawa H 1990 *Phys. Rev.* B **41** 9168
[32] Scalapino D J, White S R and Zhang S C 1992 *Phys. Rev. Lett.* **68** 2830; 1993 *Phys. Rev.* B **47** 7995
[33] Lilly L, Muramatsu A and Hanke W 1990 *Phys. Rev. Lett.* **65** 1379
Mehlig B 1993 *Phys. Rev. Lett.* **70** 2048
Lilly L, Muramatsu A and Hanke W 1993 *Phys. Rev. Lett.* **70** 2049
[34] White S R, Scalapino D J, Sugar R L, Loh E Y, Gubernatis J E and Scalettar R T 1989 *Phys. Rev.* B **40** 506
[35] Moreo A, Scalapino D J, Sugar R L, White S R and Bickers N E 1990 *Phys. Rev.* B **41** 2313
[36] Walker M B and Ruijgrok Th W 1968 *Phys. Rev.* **171** 513